ISSN 1846-6168 (Print), ISSN 1848-5588 (Online)
ID: TG-20171019175235

Original scientific paper

NUMERICAL INVESTIGATION OF THE INFLUENCE OF TIP CLEARANCE AND ROTOR-STATOR INTERACTION ON CENTRIFUGAL PUMP PERFORMANCE AND CAVITATION

Cong LIU

Abstract: The influence of tip clearance on pump performance and the impact of the rotor-stator interaction on cavitation are investigated by numerical means, respectively. Firstly, the SST model is employed in numerical anaylsis, and the numerical investigation of the pump performance based on a different turbulence model is compared with the experimental data. Secondly, the pump performance at different tip clearances is investigated, and the numerical results indicate that the smaller tip clearance the better performance of keeping the head stable at a low mass flow rate. Thirdly, as the NPSH-Head curves are computed at different tip clearances, the conclusion can be drawn that the smaller the tip clearance, the stronger the capability of preventing cavitation. Lastly, the effect of the rotor-stator interaction on cavitation is performed at a design case, when the φ = 9°, the volume fraction of cavitation is maximum, however, when the φ = 120°, the volume fraction of cavitation is minimum. Besides, the blade loading is studied at a corresponding φ value. When the φ = 44°, the blade loading is minimum, however, when the φ = 120°, the blade loading is maximum. The cavity all appears from the leading edge to the 20% chord length for a different φ value, which indicates that the cavitation zone grows along the normal direction of the suction surface.

Keywords: cavitation; radial pump; rotor-stator interaction; tip clearance

1 INTRODUCTION

The radial diffuser pump is favoured for applications in a wide range of industrial domains, such as power plants, papermaking, chemical production, and so on. It is necessary to maintain a gap between the blade tip and the stationary shroud to ensure the relative motion. However, a channel is formed for water to leak because of the gap, which will contribute to a tip leakage flow, and the flow not only has a significant effect on the head and efficiency, but may also lead to cavitation. Cavitation can cause the deterioration of pump performance, noise, vibration and wall erosion, etc. [1], which are all undesirable phenomena.

The effect of tip clearance on suction performance at different flow rates in a mixed flow pump has been investigated by Yo Han Jung, et al. [1]. For large tip clearance, the head breakdown happened earlier at the design and high flow rates, but the area size of the cavitation at different tip clearances and flow rates was not examined. The unsteady cavitation flows in the centrifugal pump was studied by Wang Jian [2] by using the improved turbulence model to predict the cavitation inception, shedding off and collapse procedures, however, the tip clearance is not considered. Some experiments [3] are conducted by changing the tip gap sizes to investigate the correlation between the cavitation inception number and tip leakage vortex in an axial flow pump. The tip leakage vortex structure and cavitation patterns in an axial flow pump are revealed by the author using an experimental and improved numerical method [4, 5].

The influence of different viscosity and incompressible gas content on cavitation in a centrifugal pump was presented by Wen-Guang Li [6], who found that the NPSHr was more easily impacted by incompressible gas content. Besides, the impact of different temperature was investigated by other researchers through an experiment and simulation [7÷10].

The impact of rotor-stator interaction on the head in a centrifugal pump is studied by Feng Jianjun [11] by using PIV and LDV, but cavitation is not considered. The experimental and numerical investigation of the processing of helical vortex in a conical diffuser with a rotor–stator interaction was carried out by A. Javadi [12]. The flow unsteadiness generated in a swirl apparatus was analysed, but the influence of rotor-stator interaction on cavitation was according to him not present.

In this paper, the performance of pump at different flow coefficients was compared between the experiment and simulation to verify the correctness of the numerical method firstly. Secondly, the effect of tip clearance on pump performance was obtained with three different tip sizes. The cavitation model was employed to get the NPSH-H curve at different tip clearance sizes and the impact of rotor-stator interaction on the volume fraction of cavitation was investigated. Lastly, the blade loading was examined and compared under different relative circumferential positions between the rotating impeller and stationary diffuser.

2 GOVERNING EQUATIONS AND THE CAVITATION MODEL

Cavitation in a pump is treated differently from the thermal phase change, because the cavitation process is too quick at the interface to be modified for the assumption of thermal equilibrium. In highly simplified cavitation models, mass transfer is only driven by mechanical effects, in other words, by the liquid-vapour pressure differences rather than the thermal. In this paper, the Rayleigh-Plesset model is implemented as an interphase mass transfer model. For the cavitation flow, the homogeneous multiphase model is normally used, so each fluid component is assumed to have the same velocity and pressure. The governing equations in

the homogeneous multiphase and the Rayleigh-Plesset equation are as follows.

Continuity Equations

$$\frac{\partial}{\partial \mathrm{t}}\left(r_\alpha \rho_\alpha\right)+\nabla \cdot\left(r_\alpha \rho_\alpha U_\alpha\right)=S_{MS\alpha}+\sum_{\beta=1}^{N_p} \Gamma_{\alpha\beta}. \tag{1}$$

Where N_p is the total number of the phase, the volume fraction of each phase is denoted by r_α, $\alpha = 1$ to N_p. The user specified mass sources are described by $S_{MS\alpha}$, and $\Gamma_{\alpha\beta}$ is the mass flow rate per unit volume from phase β to phase α. This term only occurs when the interphase mass transfer happens. In this study, as neither the mass sources nor the interphase mass transfer exist, and the total number of the phase is 2, the equation can be simplified as follows:

$$\frac{\partial}{\partial \mathrm{t}}\left(r_\alpha \rho_\alpha\right)+\nabla \cdot\left(r_\alpha \rho_\alpha U_\alpha\right)=0. \tag{2}$$

Momentum Equations

$$\frac{\partial}{\partial t}(\rho U)+\nabla \cdot\left(\rho U \otimes U_\alpha-\mu\left(\nabla U+(\nabla U)^T\right)\right)=S_M+\nabla p. \tag{3}$$

Where $\rho=\sum_{\alpha=1}^{N_p} r_\alpha \rho_\alpha$, $\mu=\sum_{\alpha=1}^{N_p} r_\alpha \mu_\alpha$. Obviously, the equation is essentially a single phase transport with variable density and viscosity, and the interphase transfer terms have all been cancelled out. Due to the external body forces, S_M describes the momentum sources; considering the radius of the pump impeller is small, the momentum sources term can be ignored.

Cavitation Model

The Rayleigh-Plesset model is implemented to model the cavitation in the centrifugal pump. It provides the basis for the rate equation controlling vapour generation and condensation. This equation describes the growth of a gas bubble in the pump and is as follows:

$$R_B \frac{\mathrm{d}^2 R_B}{\mathrm{d}t^2}+\frac{3}{2}\left(\frac{\mathrm{d}R_B}{\mathrm{d}t}\right)^2+\frac{2\sigma}{\rho_w R_B}=\frac{p_\mathrm{v}-p}{\rho_w}. \tag{4}$$

Where R_B represents the bubble radius, p is the pressure in the water surrounding the bubble, ρ_w is the density of water, and the surface tension coefficient between the water and water vapour is described by σ, p_v is the saturation vapour pressure of water at the temperature, and it is has the following empirical formula:

$$p_v=p_k \exp\left\{\left(1-\frac{T_K}{T}\right)\left[a+(b-cT)(T-d)^2\right]\right\}. \tag{5}$$

Where $p_K = 22.13$ MPa, $T_K = 647.31$ K, $a = 7.21379$, $b = 1.152\times10^{-5}$, $c = -4.787\times10^{-9}$, $d = 483.16$. In this paper, $T = 25$ °C, hence p_v can be calculated and it is 3229Pa.

Neglecting the surface tension between the water and water vapour and the second order terms, which only have a significant effect on the rapid bubble acceleration, the equation can be reduced to:

$$\frac{\mathrm{d}R_\mathrm{B}}{\mathrm{d}t}=\sqrt{\frac{2}{3}\frac{p_v-p}{\rho_w}}. \tag{6}$$

The corresponding rate of the change of bubble volume and mass are derived as follows:

$$\frac{\mathrm{d}V_\mathrm{B}}{\mathrm{d}t}=\frac{\mathrm{d}}{\mathrm{d}t}\left(\frac{4}{3}\pi R_B^3\right)=4\pi R_B^2\sqrt{\frac{2}{3}\frac{p_v-p}{\rho_w}} \tag{7}$$

$$\frac{\mathrm{d}m_\mathrm{B}}{\mathrm{d}t}=\rho_v\frac{\mathrm{d}V_\mathrm{B}}{\mathrm{d}t}=4\pi R_B^2\rho_v\sqrt{\frac{2}{3}\frac{p_v-p}{\rho_w}}. \tag{8}$$

If the bubble number per unit volume is denoted by N_B, the volume fraction of vapour, r_v, can be expressed as:

$$r_v=V_B N_B=\frac{4}{3}\pi R_B^3 N_B. \tag{9}$$

The total interphase mass transfer rate per unit volume is:

$$\dot{m}_{wv}=N_B\frac{\mathrm{d}m_B}{\mathrm{d}t}=\frac{3r_v\rho_v}{R_B}\sqrt{\frac{2}{3}\frac{p_v-p}{\rho_w}}. \tag{10}$$

Assuming bubble growth, namely vaporization, the expression can be generalized to contain condensation as follows:

$$\dot{m}_{wv}=F\frac{3r_v\rho_v}{R_B}\sqrt{\frac{2}{3}\frac{|p_v-p|}{\rho_w}}\mathrm{sgn}(p_v-p). \tag{11}$$

Where F is an empirical factor that may differ between condensation and vaporization, the reason is that the rate of vaporization is usually much faster than that of condensation. A number of studies have shown that vaporization is firstly initiated at nucleation sites, which is why the bubble radius R_B is replaced by the nucleation site radius R_nuc for simulating purposes. As the volume fraction of vapour increases, accordingly, the nucleation site density must decrease because of less liquid. For vaporization, r_v in the equation is replaced by $r_\mathrm{nuc}(1-r_v)$, where r_nuc is the volume fraction of the nucleation sites, which is why the equation for the vaporization progress is given:

$$\dot{m}_{wv}=F\frac{3r_\mathrm{nuc}(1-r_v)\rho_v}{R_B}\sqrt{\frac{2}{3}\frac{|p_v-p|}{\rho_w}}\mathrm{sgn}(p_v-p). \tag{12}$$

The Rayleigh–Plesset cavitation model adopted by CFX is validated by Bakiretal [13] and requires the following values of the two-phase flow parameters, which are appropriate for most cavitation simulations [14, 15]. The parameters are listed as follows: R_{nuc} = 1 μm, r_{nuc} = 5×10^{-4}, F_{vap} = 50, F_{cond} = 0.01.

3 SIMULATION PROCEDURE

3.1 Physical model

A radial diffuser pump with the specific speed of n_s = 82.5 is researched in this paper. The pump of flow rate, head and rotational speed are Q_d = 0.0045 m^3/s, H_d = 7 m and n_d = 1450 rpm, respectively, at a design point. The diameter of the impeller inlet and outlet are 0.08 m and 0.1505 m, the absolute flow angle is 80 degrees, and the blade number of impeller is 6. Correspondingly, 0.155 m and 0.19 m are the inlet and outlet diameters of the diffuser, the absolute flow angle is 60 degrees and the blade number of the diffuser is 9. The view of the pump is shown in Fig. 1, and Tab. 1 presents the specifications of the pump.

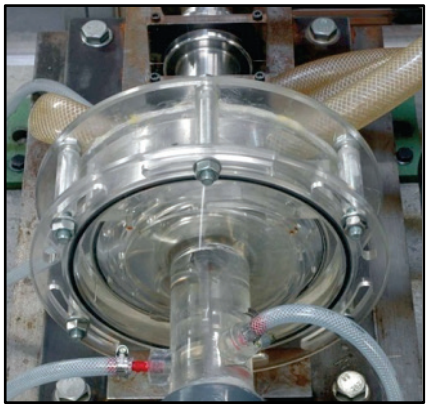

Figure 1 The view of the pump

Table 1 Specifications of the pump

Impeller parameters	Value
Number of blade Z_i	6
Impeller inlet diameter d_1 (m)	0.08
Impeller exit diameter d_2 (m)	0.1505
Absolute flow angle α_i (°)	80
Blade inlet angle β_{1i} (°)	17.9
Blade outlet angle β_{2i} (°)	22.5
Blade span b_i (m)	0.0127
Diffuser parameters	
Number of vanes Z_d	9
Diffuser inlet diameter d_3 (m)	0.155
Diffuser outlet diameter d_4 (m)	0.19
Absolute flow angle α_d (°)	60
Vane inlet angle β_{1d} (°)	171
Vane outlet angle β_{2d} (°)	160.3
Vane span b_d (m)	0.014
Design operating conditions	
Impeller rotational speed n (rpm)	1450
Specific speed n_s	82.5
Flow rate Q_d(m^3/s) Q_d (m^3/s)	0.0045
Delivery head H_d (m)	7

3.2 Computational model and boundary conditions

With the assumption that the flow is in the incompressible steady state, the internal flow of the pump is simulated by using the CFX software. Because of the rotation of the impeller, the MRF (multiple frame of reference) is selected, and the interface type between the impeller outlet and diffuser inlet adopts the frozen rotor model. The geometry of the pump to be modelled includes two impeller blade passages and three diffuser blade passages, because the frozen rotor model requires the pitch ratio at the interface between the impeller and diffuser to be 1 for as much as possible, as it considers the accuracy and reliability of the numerical result. The Counter Rotating Wall is adopted by the shroud of the impeller, and the blade wall and hub are set to a no slip boundary. Besides, the diffuser is stationary. Periodic boundaries are used to enable only 1/3 of the section of the full pump geometry to be modelled.

Three turbulence models are compared with the experimental data. The data carried out by the k-ω based on SST (Shear Stress Transport) model has a better agreement with the results of the experiment than the others, as shown in Fig. 2, which is why the k-ω based on the SST model is employed to solve the three-dimensional steady Reynolds-averaged equations.

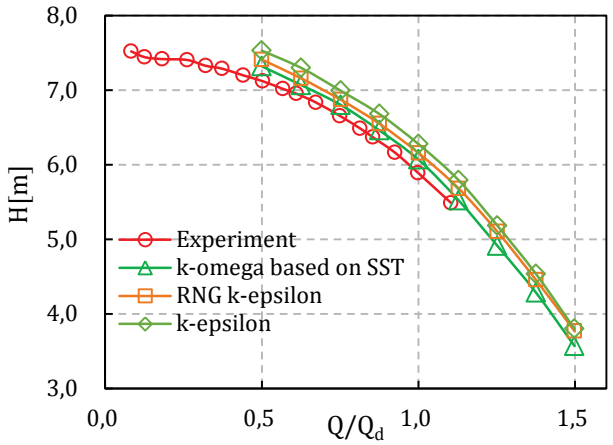

Figure 2 Head rise of the experimental and computational results

3.3 Mesh generation and independence verification

The high resolution structured hexahedral mesh has been generated for a computational domain by using the ANSYS Turbo Grid 17.0 with an ATM (Automatic Topology and Meshing) option (see Fig. 3(a)). Near a no-slip wall, viscosity has a large effect on the transport processes, and there are strong gradients in the dependent variables. Besides, the SST model requires a high resolution of the boundary layer of more than 10 points, which is why an O-Grid is built and refined to satisfy the requirements for the surrounding of the blades [16]. The wall-normal mesh resolution unit y^+ is defined as [17]

$$y^+ = u^* y/\nu,\ u^* = \sqrt{\tau_w/\rho},\ \tau_w = \mu\left(\frac{\partial u}{\partial y}\right), \quad (13)$$

where u^* is the friction velocity and τ_w is the wall shear stress. The mean value of y^+ is controlled below 10 in the surrounding of the impeller blade and diffuser vane when using the SST, and the mesh resolution is acceptable, while an H-Grid is applied for the passage. The detailed mesh information near the leading and trailing edges of the impeller blades and diffuser vanes are enlarged in Fig. 3(b), 3(c), respectively.

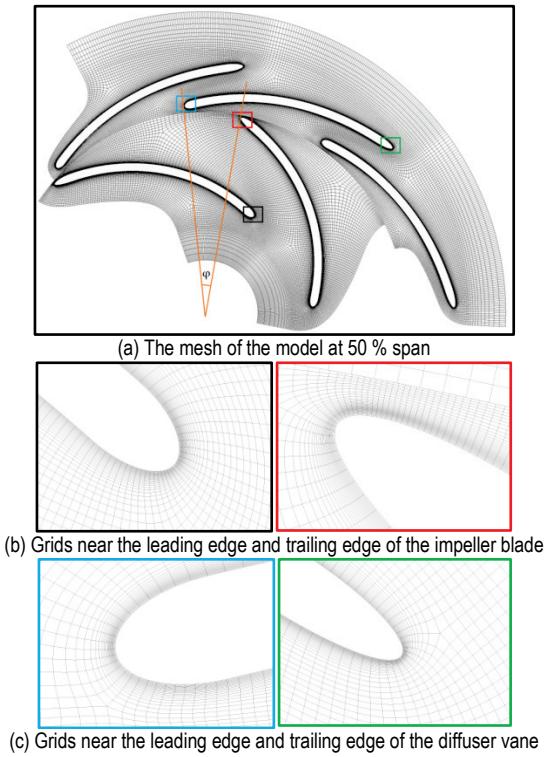

(a) The mesh of the model at 50 % span

(b) Grids near the leading edge and trailing edge of the impeller blade

(c) Grids near the leading edge and trailing edge of the diffuser vane

Figure 3 The mesh of the computational domain

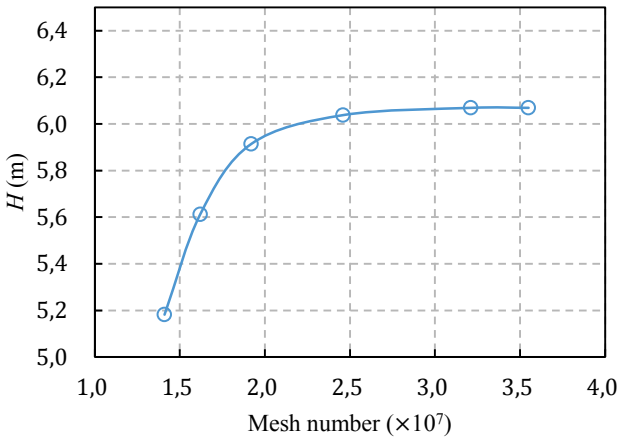

Figure 4 Independence verification of the mesh number

To eliminate the effect of the mesh number upon the numerical results, the independence verification of the mesh is carried out with six different numbers of the mesh. When the mesh number exceeds 3.21×10^7, as shown in Fig. 4, the numerical results remain almost unchangeable. Thus, the mesh number of 3.21×10^7 meets the requirement of calculating accuracy and is selected in this study.

3.4 Solutions

The high resolution option was chosen for the advection scheme and turbulence numerics. The results implementing the first order scheme will be used as the initial value of the high resolution scheme in case the scheme is not robust. When the RMS (root mean square) residual value is less than 10^{-4}, and the volume flow rate difference between the inlet and outlet reaches 10^{-5} simultaneously, the calculation will be terminated and considered to have converged.

In this paper, the effect of three different tip clearance sizes on the performance of the pump and cavitation will be studied, as shown in Tab. 2, 0.6 mm, 1.3 mm and 2.0 mm, respectively. Besides, the influence of a relative circumferential position between the rotating impeller and stationary diffuser on cavitation is obtained.

Table 2 Numerical simulate cases

Simulation case	Tip clearance size
Case 1	0.6 mm
Case 2	1.3 mm
Case 3	2.0 mm

4 RESULTS AND DISCUSSIONS

4.1 The effect of variation in tip clearance on pump performance without cavitation

Fig. 5 provides the performance of the pump at different tip clearances and a different mass flow rate. The figure exhibits that the head of the pump decreases as the tip clearance increases. Keeping the head in view, when the mass flow rate is less than 1, the rate of the head increase will decrease with the decrease of tip clearance. Moreover, at the same mass flow rate, the increase of the head from the tip clearance of 2.0 mm to 1.3 mm is less than from 1.3 mm to 0.6 mm. However, when the mass flow rate is more than 1, the relation is not remarkable, but the head of all tip clearances decreases as the mass flow rate increases.

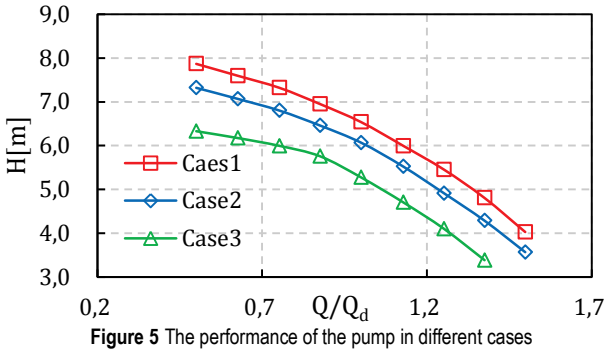

Figure 5 The performance of the pump in different cases

From the results of the simulation, what can be observed is the characteristic that a smaller tip clearance has a better performance of keeping the head stable than a

bigger tip clearance at low mass flow rate. However, it is extraordinarily difficult to keep a clearance of less than 0.5 mm, so the size of tip clearance is limited.

4.2 The effect of variation in tip clearance on pump cavitation performance at a design mass flow rate

Fig. 6 shows pump cavitation performance in the form of curves, which is a chart of the head vs. NPSH (Net Positive Suction Head) at a design mass flow rate under different tip clearances, where NPSH is defined as the pressure differential between the liquid total pressure of the pump inlet and the saturated vapour pressure at a pumping temperature [18]. The NPSH is illustrated by [19].

$$NPSH = \frac{P_{\text{tin}} - P_v}{\rho_l g} \tag{14}$$

As shown in Fig. 6, for a part of the simulation, the degradation in the NPSH vs. head curves with the reduction of the pump inlet total pressure is not significant. This is due to the fact that the pump inlet total pressure is significantly high to impede cavitation, namely, the normalized pressure rise through the pump is almost constant. However, with the pump inlet pressure dropping progressively, the incipient cavitation will emerge but will have little impact on the performance of the pump. Until the blade passage has enough blockage due to the vapour, the performance will rapidly degrade.

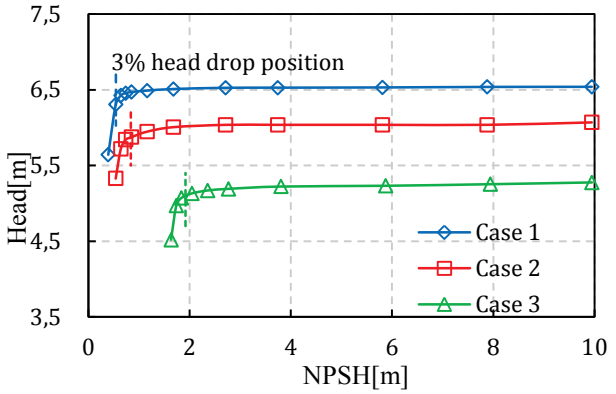

Figure 6 The drop curves of the NPSH vs. head at a design mass flow rate under different tip clearances

As the tip clearance decreases, the head breakdown corresponding to the 3 % head drop emerges at a smaller NPSH value, which demonstrates that the smaller the tip clearance, the stronger the capability of preventing cavitation. However, the relationship between the increase of the tip clearance and enhancement of the capability of preventing cavitation is nonlinear.

4.3 The effect of rotor-stator interaction on cavitation

The transient blade row modelling and cavitation model were employed to investigate the influence of the relative circumferential position between the rotating impeller and stationary diffuser on cavitation. The rotating angle φ indicated the relative circumferential position between the rotating impeller and stationary diffuser, and φ = 0 degree is defined when the prescribed impeller blade trailing the edge approaches the designated diffuser vane leading the edge (Fig. 3(a)).

In order to analyse the effect of rotor-stator interaction on cavitation, the volume fraction of cavitation (VFC) is defined below.

$$VFC = \frac{V_c}{V_p} \times 100\%, \tag{15}$$

where V_c is the volume of zone, whose pressure is below 3229Pa. V_p is the total volume of the computational domains.

Fig. 7 shows the relation of VFC and the head with φ at a 3 % head drop point of the case 2. The head profiles at φ = 0 degree show a very good periodicity for each 120 degrees, obviously, within the circumferential range of 360 degrees. The average of the head under the condition of the unsteady is equal to the steady, which validates the expected flow correctness for the numerical simulation.

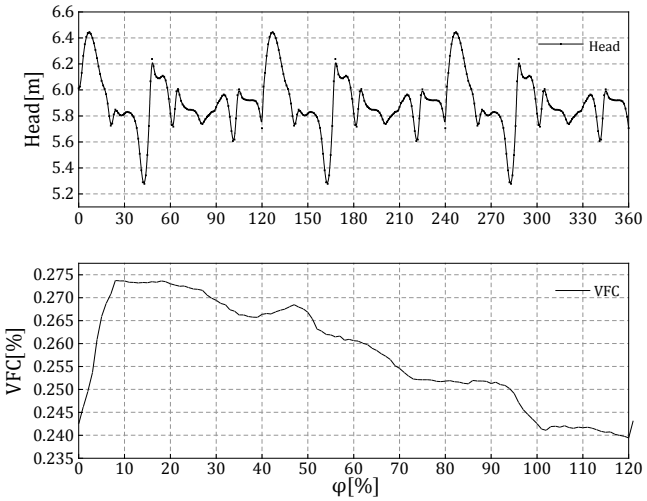

Figure 7 Head and VFC compared with different φ at a 3 % head drop point of the case 2

As Fig. 7 shows, the head has relative fluctuation amplitude of about 8÷10 % with the impeller position φ. Both the head and VFC have extreme points at the same φ value. However, the VFC shows the trend of falling down. When φ = 9°, VFC reaches the maximum value, about 0.27 %, and correspondingly, the head also achieves the maximum value, about 6.45 m. As the impeller rotates, the head reaches the minimum value, about 6.43 m, at φ = 44°. When the VFC reaches the minimum value, about 0.24 %, at φ = 120°, the head reaches the minimum value, about 5.7 m.

4.4 The blade loading at different φ values

The static pressure on the suction and pressure that surfaces at a 50 % span was estimated for different φ values at a 3 % head drop point of the case 2. The variation of the static pressure is shown in Fig. 8.

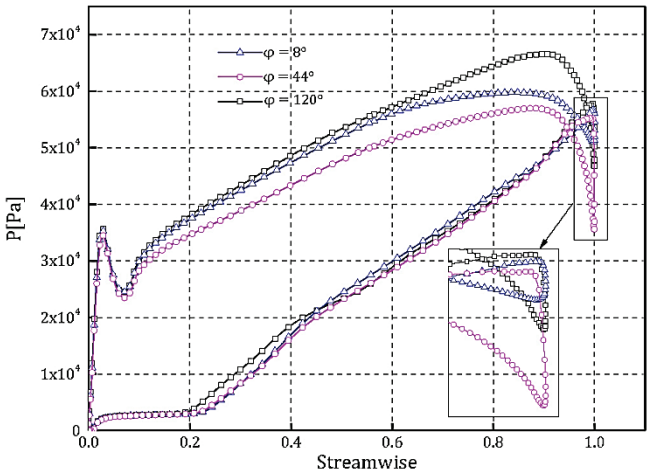

Figure 8 The blade loading at different φ values at a 3 % head drop point of the case 2

The blade loading is represented by the area inside the curve, which indirectly represents the work done by the impeller. It is observed that the static pressure variation is affected by the relative position of the rotor and stator. The lowest pressure emerges on the suction side around the leading edge and almost keeps its constant value, which is equal to the vapour pressure, and then it rapidly increases. Because the cavitation bubble develops along the blade suction side within the constant pressure region, the cavity zone corresponds to this region. In fact, the cavity appears from the leading edge to the 20 % chord for different φ values, which indicates that the cavitation zone grows along the normal direction of the suction surface. As for the blade loading, when φ = 120°, the blade loading reaches a maximum, and the VFC is at its minimum value.

5 CONCLUSIONS

A simulation was carried out for the mass flow parameter ranging from 0.5 to 1.5 at a design speed using different turbulence models, and the k-ω based on the SST turbulence model was chosen eventually. Then the numerical data was compared with the experimental data. The influence of three different tip clearances on the performance of the pump were researched; the smaller tip clearance the better performance of keeping the head stable, but the size of tip clearance is limited. The pump cavitation performance on different tip clearances were studied by using the cavitation model, and the conclusion is that the smaller the tip clearance, the stronger the capability of preventing cavitation. Lastly, transient blade row modelling was employed to examine the relation between the cavitation and rotor-stator interaction. When φ = 9°, the VFC reached a maximum value, while the minimum value achieved was at φ = 120°. Meanwhile, the blade loading was also estimated, and when the blade loading reaches a maximum at φ = 120°, the VFC is at its minimum value. The cavity appears from the leading edge to the 20 % chord length, indicating that the cavitation zone grows along the normal direction of the suction surface.

6 REFERENCES

[1] Yo Han Jung, Young Uk Min, and JinYoung Kim, 2014, "Effect of tip clearance on suction performance at different flow rates in a mixed flow pump", ASME US-European Fluids Engineering Division Summer Meeting.

[2] Jian Wang, Yong Wang, Houlin Liu, Haoqin Huang, Linglin Jiang, (2015) "An improved turbulence model for predicting unsteady cavitating flows in centrifugal pump", International Journal of Numerical Methods for Heat & Fluid Flow, Vol. 25 Iss: 5, pp. 1198-1213.

[3] Laborde, R., Chantrel, P., and Mory, M., 1997, "Tip Clearance and Tip Vortex Cavitation in an Axial Flow Pump", ASME J. Fluids Eng., 119(3), pp. 680–685.

[4] Zhang D, Shi W, Pan D, Dubuisson M. Numerical and Experimental Investigation of Tip Leakage Vortex Cavitation Patterns and Mechanisms in an Axial Flow Pump. ASME.J. Fluids Eng.2015;137(12):121103-121103-14.

[5] Desheng Zhang and Weidong Shi. Study on Unsteady Tip Leakage Vortex Cloud Cavitation in an Axial Flow Pump Using an Improved Numerical Method. ASME/JSME/KSME 2015 Joint Fluids Engineering Conference. No. AJKFluids2015-33010, pp. V001T33A001; 14.

[6] Li W. Modeling Viscous Oil Cavitating Flow in a Centrifugal Pump. ASME.J. Fluids Eng.2015; 138(1):011303-011303-12.

[7] Hirschi, R., Dupont, P., Avellan, F., Favre, J. N., Guelich, J. F., and Parkinson, E., 1998, "Centrifugal Pump Performance Drop Due to Leading Edge Cavitation: Numerical Predictions Compared With Model Tests", ASME J. Fluids Eng., 120(4), pp. 705–711.

[8] Wursthorn, S., and Schnerr, G. H., 2001, "Numerical Investigation of Performance Losses in a Centrifugal Pump Due to Cavitation", ZAMM, 81(Suppl. S3), pp. S579-S580.

[9] Coutier-Delgosha, O., Patella, R. R., Rebound, J. L., Hofmann, M., and Stoffel, B., 2004, "Experimental and Numerical Studies in a Centrifugal Pump with Two-Dimensional Curved Blades in Cavitating Condition", ASME J. Fluids Eng., 125(6), pp. 970-978.

[10] K David Huang, Sheng-Chung Tzeng, Wei-Ping Ma, Effects of anti-freeze concentration in the engine coolant on the cavitation temperature of a water pump, Applied Energy, Volume 79, Issue 3, November 2004, pp. 261-273.

[11] Feng, J; Benra, F; Dohmen, H. Unsteady Flow Visualization at Part-Load Conditions of a Radial Diffuser Pump: by PIV and CFD. Journal of Visualization. 12, 1, 65-72, 2009. ISSN: 13438875.

[12] Javadi, A. et al. Experimental and Numerical Investigation of the Precessing Helical Vortex in a Conical Diffuser, With Rotor-Stator Interaction. Journal of Fluids Engineering. 138, 8, 1, Aug. 2016. ISSN: 00982202.

[13] F. Bakir, R. Rey, A.G. Gerber, T. Belamri and B. Hutchinson, Numerical and Experimental Investigations of the Cavitating Behavior of an Induce, Int J Rotating Machinery, Vol. 10, pp. 15-25, 2004.

[14] Tang, F., and Li, J. W., 2010, Numerical Simulation of Rotating Cavitation in a Liquid Hydrogen Pump Inducer,

Proceedings of the 13th Asian Congress of Fluid Mechanics, Dhaka, Bangladesh.
[15] Ding, H., Visser, F. C., Jiang, Y., and Furmanczyk, M., 2011, Demonstration and Validation of a 3D CFD Simulation Tool Predicting Pump Performance and Cavitation for Industrial Applications, ASME J. Fluids Eng., 133(1), p. 011101.
[16] Bardina, J. E., Huang, P. G. and Coakley, T. J., Turbulence Modeling Validation Testing and Development, NASA Technical Memorandum 110446, 1997.
[17] Javadi, A; et al. Experimental and Numerical Investigation of the Precessing Helical Vortex in a Conical Diffuser, With Rotor-Stator Interaction. Journal of Fluids Engineering. 138, 8, 1, Aug. 2016.
[18] Li W. Modeling Viscous Oil Cavitating Flow in a Centrifugal Pump. ASME. J. Fluids Eng. 2015; 138(1):011303-011303-12. doi:10.1115/1.4031061.
[19] Brennen, C. E., 1994, Hydrodynamics of Pumps, Oxford University Press, Oxford.

Author's contacts:

Cong LIU,
Xuhai College, China University of Mining and Technology,
No. 1 Jinshan East Road, Quanshan District
221000 Xuzhou, Jiangsu Province, China
Tel./Fax: +8615152101093
E-mail: 511070388@qq.com